PERFORMANCE OF THE LOS ALAMOS EXPANDING TELESCOPE*

T. Dombeck
On Behalf of the Los Alamos-Argonne Collaboration
Los Alamos National Laboratory, Los Alamos, NM
87545, USA

Abstract

An expanding telescope can produce a very low divergence particle beam, provided that the beam optics have sufficient quality in order not to introduce large aberrations. Even as late as two years ago, most beamline designs were carried out using first-order computer codes, and there existed little experimental work to describe the third-order aberrations introduced by an expanding telescope. A project was undertaken at Los Alamos National Laboratory to perform these calculations, and to build a telescope to confirm the predictions. It was installed at Argonne National Laboratory during the summer of 1987 and tested with a 50 MeV H^- beam. The telescope consisted of a singlet eyepiece and triplet objective lens with a twenty times magnification. It performed to the design specifications of twenty-five microradians rms beam divergence with a parallel focus. The measured geometric aberrations were found to be in agreement with the computer calculations.

Beamline, Telescope, and Diagnostics Equipment

The experiment was performed using the Argonne Laboratory 50 MeV H^- linear accelerator. The rms momentum spread of the beam incident into the telescope was measured to be less than 0.1%. The beam emittance was adjusted using collimators in the transport line between the accelerator and the telescope to yield the desired rms value close to 0.06 π-cm-mrad. With these settings we achieved a beam current near 250 microamps incident on the telescope at a 3 Hz pulse rate. Due to the low current densities, space-charge effects were negligible throughout the experiment.

The telescope is shown schematically in Fig. 1. and consisted of a singlet eyepiece and a triplet objective lens, each composed of permanent magnets. The overall length between the centers of the magnetic elements was 7.7 meters. The design magnification was twenty, providing a Gaussian-shaped profile with a 2.5-cm rms radius at the telescope exit. The beamline and telescope parameters are summarized in Table I.

TABLE I. BEAMLINE AND TELESCOPE PARAMETERS

Beam	50 MeV H^-
Momentum spread	< 0.1% (rms)
Emittance	0.06 π-cm-mrad (rms)
Telescope length between magnet centers	7.7 m
Eyepiece	quadrupole singlet (permanent magnet)
Objective lens	quadrupole triplet (permanent magnets)
Objective lens aperture	0.3 m
Telescope magnification	20 x
Output spot size	2.5-cm radius (rms)
Output beam divergence	< 25 microrad (rms)
Stripline beam position monitor resolution	± 45 microns
Wire scanners:	
wire size	50-micron diameter (Ni)
position resolution	± 20 microns
Wire harps:	
wire spacing	30 wires spaced 5 mm apart
wire size	500 microns wide by 12 microns thick (Ni)

The telescope diagnostics included a toroid, stripline beam position monitors, wire scanners, fluorescent screens, and wire harps. The positions of each of these devices is indicated in Fig. 1, and their sensitivities are summarized in Table I. These devices were used to align the beam and to obtain the correct focus to a level near an rms of 400 microradians/cm.

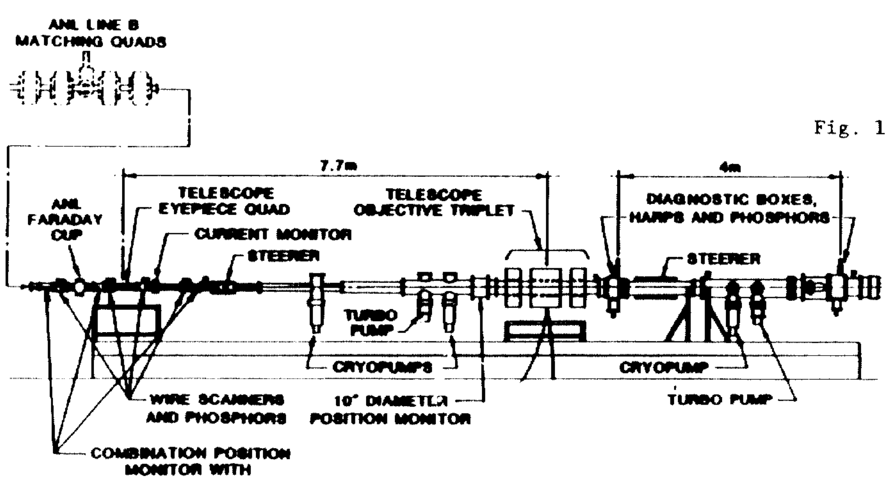

Fig. 1. The expanding telescope for the 50 MeV H^- beam is shown schematically. The eyepiece and objective lens were composed of permanent magnets. The positions of the telescope diagnostics are also indicated. The parameters of the telescope elements are summarized in Table I.

Beam Characterization Equipment

The telescope had a design specification of twenty-five microradians beam divergence with a parallel beam focus. Angular distortions in the beam introduced by the geometric aberrations were parametrized by [1]:

$$\theta(x,y) = Ax + Bx^3 + Cxy^2$$

$$\phi(x,y) = Dy + Ey^3 + Fx^2y \qquad (1)$$

The first order terms in (1) gave a measure of the beam focus, while the cubic and cross terms gave a measure of the third-order aberrations. The aberration coefficients, determined by computer calculations [1] using the telescope parameters, predicted a distortion in the beam of a few microradians per cm^3, giving rise to angular deviations of up to 250 microradians at twice the rms beam radius. The characterization of the telescope optics at this precision required measurements in a range that had seldom, if ever, been achieved for a particle beam.

An optical method of imaging pinholes onto a fluor was developed to measure the beam quality out of the telescope. The equipment is shown schematically in Fig. 2, and was placed just downstream of the telescope objective lens. A plate with tiny pinholes was inserted into the expanded beam in diagnostics box DB02 just downstream of the steering magnet. The incident H^- particles were stripped to H^+ everywhere in the plate except where the tiny pinholes intercepted the beam. The pinholes, having diameters of about 200 microns, were coated with a thin neutralizer foil, 8 micrograms/cm^2 in areal density, that converted half of the remaining H^- to neutral H^0. A large sweep magnet downstream of the pinhole plate removed all charged species leaving only the neutral H^0 beamlets to continue downstream.

The pinhole beamlets travelled to a fluorescent screen placed at a distance Z of 10 meters. The pinholes were arranged in a rectilinear array on 1-cm centers, such that distortion caused by the beam aberrations appeared as shifts in the centroids of the images from their expected positions:

$$\theta = (x(\text{fluor image position}) - x(\text{pinhole position}))/Z$$

$$\phi = (y(\text{fluor image position}) - y(\text{pinhole position}))/Z. \qquad (2)$$

These measurements were related to the aberration coefficients using (1). In propagating over the 10-m distance, the beamlets also grew in diameter, such that the observed pinhole widths also provided a measure of the intrinsic beam divergence.

The pinhole images were viewed on RAREX (BG-fine and medium) fluors. Two cameras recorded the pinhole images in the detector chamber. One of these employed a cooled charged-coupled device (CCD) with a 27 micron pixel size on a grid of 512 rows by 512 columns. This camera viewed the entire beam spot (about a 10-cm diameter viewing area) with a magnification near 0.1. It was used to obtain information on beam focus and aberrations. The other camera was an 18-mm FPS videcon placed on the opposite side of the beamline. It was used at a magnification near unity, such that it imaged the width of individual pinholes to obtain a measure of the beam divergence. Either camera could be used by moving the appropriate mirror and fluor into place. This procedure did not require re-focus or re-calibration of the cameras. A calibration plate, inserted at the fluor position, was used periodically to check the geometric integrity of the CCD and videcon cameras.

A second optical method to characterize the beam used a precision grid of wires placed directly in the H^- beam (in diagnostics box DB01). The grid cast shadows onto a fluor at a distance of 4.5 meters (in DB02). The grid wires were positioned at 5-mm intervals and the wire locations were measured to a one micron precision. The Ni wires used in the grid were 250 microns wide. The shadow images were viewed on a RAREX fluor by a CCD camera (11.5-micron x 27-micron pixel size), placed at a 30° angle with respect to the beam axis. The camera pan, tilt and focus were adjusted remotely.

The parameters of the pinhole and wire shadow beam characterization equipment are summarized in Table II. A direct comparison was made between the wire shadow and the pinhole measurements to see if they gave the same results for beam divergence and aberrations.

Data and Results

We tuned the telescope in steps during the run. In the first step, we adjusted quadrupole magnets in the transport line to achieve the desired spot size at the exit of the telescope and a roughly parallel beam focus. The spot size was measured

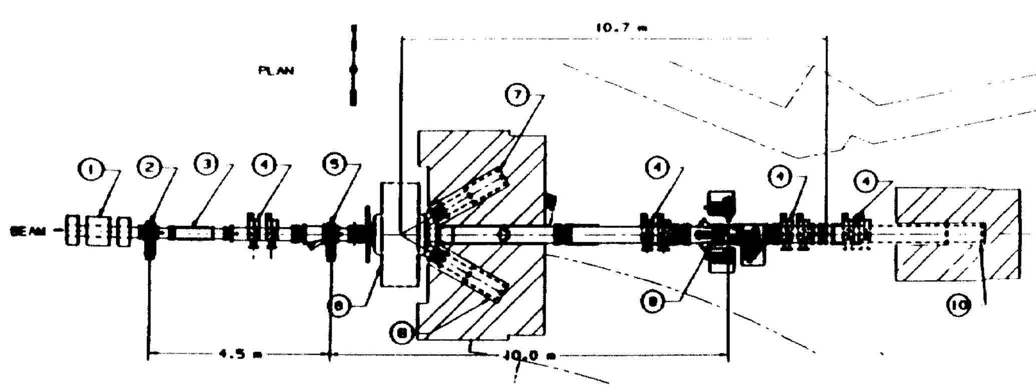

Fig. 2. The beam elements just downstream of the objective lens to the beam stop that were used for beam characterization are shown schematically. The significant parts of the line are numbered and identified in the figure, while their operation is discussed in the text.

using the wire harps, and we used wire shadows to achieve a beam focus parallel to within 100 microradians/cm by visual inspection of the average wire separation on the fluor image.

TABLE II. CHARACTERIZATION EQUIPMENT

Pinhole diagnostic:	
pinhole widths	200 microns
pinhole array	12-cm x 12-cm array on 1-cm centers
distance from pinholes to fluor	10 m
CCD camera	512 x 512 array of 27 micron pixels, magnification = 0.1
FPS videcon camera	18 mm x 18 mm active area, with 30 micron pixels, magnification = 1.0
Wire shadow diagnostic:	
wire grid	20-cm x 20-cm array on 5-mm centers
wire size	250 micron diameter (Ni)
wire spacing tolerance	measured to 1 micron
distance from grid to fluor	4.5 m
CCD camera	11.5-micron x 27-micron pixels, viewing fluor at 30^{o}, magnification near 0.1 (adjustable)

The final beam focus required small adjustments to the currents in three quadrupole trim coils wound around the beam pipe inside the permanent-magnets of the triplet objective lens. For this measurement we used a computer analysis to fit the pinhole image separations given by (2) to determine the first-order terms in (1). Using this data, the trim-coil current settings to achieve a parallel beam were calculated using theoretical values of the first-order matrices for the telescope elements. This required the solution of a set of simultaneous linear equations, which was accomplished in an iterative fashion, using the pinhole measurements and an on-line feedback program in an automatic closed-loop to adjust the trim coils. In this way we achieved a focus of ≤ 5 microradians/cm over the beam spot after about five iterations. In the final series of adjustments, the changes to the magnet field strengths amounted to only 0.1%. It should be emphasized that these magnetic field changes had to be calculated by computer, as it was virtually impossible to arrive at these settings by manual adjustment.

With the telescope at its best tune, we measured the geometric aberrations. Fig. 3 shows one of the pinhole-pattern images taken during the run. The third-order aberration is evident in the barrel distortion, and the (X,Y) centroids were again fit using (1) and (2) to obtain the aberration coefficients. Averaging over many such pictures, we obtained the third-order aberration coefficients given in Table III, along with their rms errors determined from the data. These errors show that our camera system measured these coefficients to a precision of from 2% to 10%. Also shown in Table III is the predictions of the various computer programs [2-4], and the agreement with the data is good.

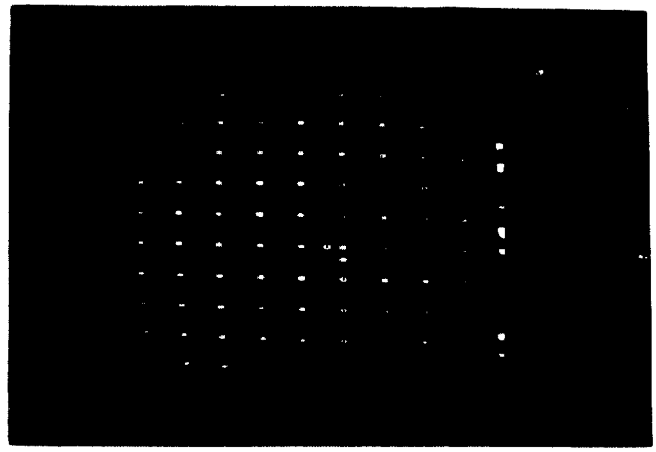

Fig. 3. A data picture taken during the run is presented showing the pinhole centroid images. The "barrel distortion" characteristic of the third-order geometric aberrations is evident. The two irregularly positioned holes in the middle of the picture are markers to indicate the center of the pinhole plate.

TABLE III. COMPARISON OF ABERRATION RESULTS FROM THE PINHOLE MEASUREMENTS WITH THOSE OBTAINED FROM THIRD-ORDER COMPUTER CODES

Coefficient	Measurement*	MARYLIE[2]	GIOS[3]	MOTR[4]
θ/X^3	-0.59 ± 0.06	-0.47	-0.51	-0.54
θ/XY^2	-2.16 ± 0.04	-2.28	-2.38	-2.34
ϕ/Y^3	-1.33 ± 0.02	-1.36	-1.39	-1.23
ϕ/YX^2	-1.97 ± 0.04	-2.28	-2.39	-2.31

References

*Work performed under the auspices of the U. S. Department of Energy and supported by the U. S. Army Strategic Defense Command.

[1] L. Schweitzer, C. T. Mottershead, and E. Heighway, "The Functional Dependence of Particle Divergence (X',Y') on Position (X,Y) at the Output of an Expansion Telescope as Simulated by the Third Order Code MARYLIE," Los Alamos National Laboratory Technical Note AT-3:87-22 (July, 1987).

[2] A. Dragt, The MARYLIE Program, University of Maryland.

[3] H. Wollnik, The GIOS Program, University of Gissen.

[4] A. Thiessen, The MOTR Program, Los Alamos National Laboratory.